Impact of Trifluoromethylation of Adiponitrile on Aluminum Dissolution Behavior in Dinitrile-Based Electrolytes

Kristina Oldiges,[1,2] Natascha von Aspern,[1,2] Isidora Cekic-Laskovic,[1] Martin Winter,[1,2,3,*] and Gunther Brunklaus[1,2,z]

[1]*Helmholtz Institute Münster, IEK-12, Forschungszentrum Jülich GmbH, 48149 Münster, Germany*
[2]*Institute of Physical Chemistry, University of Münster, 48149 Münster, Germany*
[3]*MEET Battery Research Center, 48149 Münster, Germany*

Aluminum dissolution behavior of adiponitrile (ADN) and its trifluoromethylated derivative 3-(trifluoromethyl)adiponitrile (ADN-CF_3) as single or co-solvent with propylene carbonate (PC) was determined in electrolytes with lithium bis(trifluoromethylsulfonyl) imide (LiTFSI) as conducting salt via selected electrochemical, spectroscopic and physicochemical methods. ADN-CF_3 is introduced as a promising electrolyte solvent affording reduced aluminum dissolution in the presence of imide salts. In cases where neither electrolyte components nor decomposition products thereof enable the formation of protective surface layers on aluminum current collectors, both the viscosity and relative permittivity of the solvents could be identified as key parameters for reducing aluminum dissolution. High viscosities reduce the mobility of involved species yielding increased complex formation of Li^+ and $TFSI^-$ ions or solvent molecules, hindering a reaction of $TFSI^-$ anions with the passivating aluminum oxide surface to $Al(TFSI)_x$. Low relative permittivity yields lesser ionic dissociation of the lithium salt and lower solubility of $Al(TFSI)_x$ species in viscous electrolytes. Hence, reduced aluminum dissolution was observed by substituting electrolyte solvents from PC to ADN to ADN-CF_3. The obtained results significantly contribute to better understanding of anodic aluminum dissolution behavior, while encouraging future design of advanced electrolytes with high viscosities and low-permittivity solvents that possess high oxidative stabilities.
 [DOI: 10.1149/2.0461816jes]

Manuscript submitted September 20, 2018; revised manuscript received November 6, 2018. Published December 7, 2018.

The demand for high power and energy density lithium-ion batteries (LIBs) is continuously increasing, especially for use in electric vehicles (EVs) and hybrid electric vehicles (HEVs).[1–4] High energy densities can be achieved by cathode materials that operate at high voltages (~5 V). However, current state-of-the-art non-aqueous aprotic electrolytes, consisting of organic carbonates such as ethylene carbonate (EC) and dimethyl carbonate (DMC) with lithium hexafluorophosphate ($LiPF_6$) as conducting salt, cannot be used with high voltage cathode materials, such as $LiNi_{0.5}Mn_{1.5}O_4$ (LNMO) (~5 V), due to limited oxidative stability.[5] Also, organic carbonate-based solvents possess a limited operational safety due to their high flammability and volatility, while $LiPF_6$ as typically employed conducting salt decomposes at elevated temperatures and higher voltages and is very sensitive to water thus producing the highly dangerous hydrogen fluoride (HF).[6–9] This is the reason why $LiPF_6$-based electrolytes form insoluble aluminum fluoride (AlF_3) that passivates the aluminum current collector and suppresses aluminum dissolution at high potentials.[10–13] However, aforementioned electrolyte formulations also show aluminum dissolution to a minor extent, especially recognizable after long-term cycling.[14–16] These well-known drawbacks require continuous efforts for the tailored design of electrolyte components (lithium salts, solvents or additives), i.e. future development of rather safe, non-flammable, thermally and electrochemically stable electrolytes that are compatible with high-voltage cathode materials.

Lithium bis(trifluoromethylsulfonyl) imide (LiTFSI) was selected as an alternative conducting salt, due to its superior thermal and electrochemical stability and inertness to water compared to $LiPF_6$.[17] However, in contrast to $LiPF_6$, LiTFSI causes severe aluminum current collector dissolution. The C-F bonds of $TFSI^-$ are too stable to be oxidized, yielding soluble $Al(TFSI)_x$ species instead of passivating AlF_3.[18–20] This may be circumvented by using electrolyte additives like HF,[21] lithium bis(oxalate)borate (LiBOB)[22] or lithium difluoro(oxalate)borate (LiDFOB),[23] which enable a formation of a passivation layer. In order to avoid decomposition of electrolyte components and consequently changes in electrolyte compositions, ceramic coatings[24] or solvents with low relative permittivities for reducing the solubility of the $Al(TFSI)_x$ species[25] can be applied. Yamada et al.[26] reported that high salt concentrations (>5 mol/L lithium bis(fluorosulfonyl)imide (LiFSI) in acetonitrile) may also prevent aluminum dissolution, as in this case, solvent molecules are coordinated to Li^+, and the $Al(FSI)_x$ complex hardly dissolves in the absence of "free" solvent molecules, thereby forming a stable passivation layer on the aluminum surface. This finding could be verified by Heckmann et al. for dual-ion batteries.[27] In the case of ionic liquids, Kühnel et al.[28] were able to show that $Al(TFSI)_3$ has a reduced solubility in 1-butyl-1-methylpyrrolidinium bis(trifluoromethylsulfonyl)imide ($Pyr_{14}TFSI$) compared to propylene carbonate (PC). Also on the basis of ionic liquids, Meister et al.[29] described that aluminum dissolution is more pronounced in solvents with high relative permittivities, low oxidative stabilities as well as at elevated temperatures. In general, ionic liquids and also dinitriles were suggested as suitable solvents to suppress aluminum dissolution.[30,31]

Apart from this, aliphatic dinitriles NC-$(CH_2)_n$-CN with n = 3–8 have recently been identified as promising solvents due to their good physicochemical properties, i.e., high thermal and anodic stabilties.[31–36] In terms of safety, the high flash and boiling points render these electrolytes interesting for large-scale applications, such as stationary energy storage systems. Moreover, due to the wide electrochemical stability windows (ΔE > 6 V vs. Li/Li^+),[32] the electrolytes are promising for high voltage operation, allowing application of high-voltage cathodes. Because of possessing electron-rich cyano groups, dinitriles represent promising donor solvents with good solvating properties, as well. They are relatively low in price and can be purchased with high purity,[37] though the incompatibility with graphite anodes due to insufficient formation of a solid electrolyte interphase (SEI)[38] requires the presence of co-solvents,[31,33] SEI forming additives or utilization of alternative anode materials. Farhat et al.[37] successfully cycled cells with 1 M LiTFSI in adiponitrile (ADN) as electrolyte using $Li_4Ti_5O_{12}$ (LTO) and $LiNi_{1/3}Co_{1/3}Mn_{1/3}O_2$ (NMC111) as electrodes, offering a safe and stable system with high energy density. ADN was investigated as single and co-solvent by other researchers,[31,36,39] as well, as it shows together with glutaronitrile (GLN) the best thermal and physicochemical properties of all dinitrile solvents. As ADN was pointed out as rather promising solvent for lithium-ion batteries, it will be subject of this work. Nevertheless, dinitriles do not suppress aluminum dissolution completely, but only slow down the process.[30] Abu-Lebdeh et al.[31] proposed that, with 1 M LiTFSI in ADN as electrolyte, the aluminum gets passivated by the cyano groups present

*Electrochemical Society Fellow.
[z]E-mail: g.brunklaus@fz-juelich.de

in the nitrile structure through their lone electron pair, whereas Garcia et al.[40] suggested that an insoluble product, probably comprised of Al^{3+} and $TFSI^-$ ions, is formed. However, the formed protection layer is not sufficiently stable to avoid aluminum dissolution.

ADN was modified to better understand molecular details of aluminum dissolution of dinitrile-based electrolytes, including solubility of $Al(TFSI)_x$ species and its correlation with ion transport properties. A CF_3 group[41,42] was introduced considering its effect on the aluminum dissolution behavior since the group leads to significant changes of electron density distribution within the molecule and a higher molecular mass. After synthesizing 3-(trifluoromethyl)adiponitrile (ADN-CF_3), the aluminum dissolution behavior of electrolytes containing 1 M LiTFSI as conducting salt and ADN or ADN-CF_3 as single and co-solvent with PC was investigated by means of cyclic voltammetry (CV) and chronocoulometry (CC), scanning electron microscopy (SEM), as well as X-ray photoelectron spectroscopy (XPS) analysis. Inductively coupled plasma optical emission spectrometry (ICP-OES), permittivity, viscosity, conductivity, Raman and Pulsed Field Gradient Nuclear Magnetic Resonance (PFG NMR) measurements served to better understand the aluminum dissolution behavior of the investigated electrolytes. The solubility of $Al(TFSI)_3$ in PC-, ADN- and ADN-CF_3-based electrolytes was analyzed by means of impedance measurements.

Experimental

Materials.—LiTFSI (BASF, battery grade) and LiBOB (BASF, 98.0%) were dried under vacuum ($\sim 10^{-8}$ mbar) at 120°C and 110°C, respectively. PC (BASF, battery grade), ADN (Sigma-Aldrich, 99.0%), LiFSI (Lonza, 99.0%) and 1 M $LiPF_6$ in EC/DMC (1:1 by wt) (BASF, battery grade) were used as received. The electrolytes were prepared in an argon-filled glove box using 1 M conducting salt. 3-(Trifluoromethyl)adiponitrile was obtained via a three-step synthesis route based on a procedure published by Zalesskaya et al. in 1980 (Figure 1).[43] The synthesis of $Al(TFSI)_3$ was performed as described in a patent of Earle et al. from 2006.[44]

Synthesis of 3-(trifluoromethyl)hexanedioic acid (2).—Nitric acid (70%, 40 mL, 56.5 g, 0.897 mol, 7.5 eq.) was added under argon to a mixture of ammonium metavanadate (0.1 g, 0.001 mol, 0.01 eq.) and copper powder (0.1 g, 0.001 mol, 0.01 eq.). After stirring the mixture at 60°C for 15 min, a *cis*- and *trans*-mixture of 4-(trifluoromethyl)cyclohexanol (1) (98%, 20.0 g, 0.119 mol, 1 eq.) was slowly dropped to the solution (~5 h). The solution was stirred at 70°C for 2 $\frac{1}{2}$ h and was stored in the fridge overnight. The supernatant blue liquid was decanted and the solid was dissolved in dichloromethane (30 mL). After drying the solution over magnesium sulfate, the solvent was removed under vacuum ($\sim 10^{-3}$ mbar). Dichloromethane (10 mL) was added again and the solution was stored in the fridge for 3 days. The supernatant liquid was decanted and the rest of the solvent was removed under vacuum ($\sim 10^{-3}$ mbar). 3-(Trifluoromethyl)hexanedioic acid 2 was obtained as a white solid (yield = 24.2 g, 0.113 mol, 95%). ^{1}H NMR (400 MHz, CD_3CN) [ppm]: δ = 9.30 (s, 2H, OH), 2.83-2.72 (m, 1H, CH), 2.60-2.38 (m, 4H, CH_2CH_2), 1.76/1.58 (2x sext, $J_{H\text{-}F}$ = 7.2 Hz/ 7.4 Hz, 2 × 1H, CH_2). ^{13}C NMR (101 MHz, CD_3CN) [ppm]: 173.95 (s, CH_2**C**OOH), 172.22 (s, CH_2CH_2**C**OOH), 257.19 (d, $J_{C\text{-}F}$ = 279.1 Hz, CF_3), 39.18 (q, $J_{C\text{-}F}$ = 26.2 Hz, CH), 32.57 (q, $J_{C\text{-}F}$ = 2.8 Hz, CH_2**C**H_2COOH), 30.58-30.56 (m, **C**H_2COOH), 23.58 (q, $J_{C\text{-}F}$ = 2.6 Hz, **C**H_2CH_2COOH). ^{19}F NMR (376 MHz, CD_3CN) [ppm]: δ = −71.91 (d, $J_{F\text{-}H}$ = 9.3 Hz, 3F, CF_3). ^{19}F{H} NMR (376 MHz, CD_3CN) [ppm]: δ = −71.91 (s, 3F, CF_3).

Synthesis of 3-(trifluoromethyl)hexanediamide (3).—3-(Trifluoromethyl)hexanedioic acid (2) (24.2 g, 0.113 mol, 1 eq.) and thionyl chloride (121 mL, 198.4 g, 1.668 mol, 14.8 eq.) were refluxed under argon at 100°C for 2 h. The excess thionyl chloride was thereafter removed by distillation. The acid chloride was slowly added to a cooled ammonium hydroxide solution (28-30%, 363 mL) and was stirred for 4 h under ice cooling. After stirring the solution at room temperature for 30 min, the reaction mixture was poured onto ice. 3-(Trifluoromethyl)hexanediamide (3) was obtained as a white solid, which was filtrated and dried under vacuum ($\sim 10^{-3}$ mbar) (yield = 18.5 g, 0.087 mol, 77%). ^{1}H NMR (400 MHz, DMSO-d_6) [ppm]: δ = 7.23 (d, $J_{H\text{-}F}$ = 198.2 Hz, 2H, CH_2CO**N**H_2), 7.05 (d, $J_{H\text{-}F}$ = 206.1 Hz, 2H, CH_2CH_2CO**N**H_2), 2.80-2.66 (m, 1H, CH), 2.34-2.12 (m, 4H, CH_2CH_2), 1.94/ 1.72 (2x sext, $J_{H\text{-}F}$ = 7.0 Hz/ 7.4 Hz, 2 × 1H, CH_2). ^{19}F NMR (376 MHz, DMSO-d_6) [ppm]: δ = −69.70 (d, $J_{F\text{-}H}$ = 9.8 Hz, 3F, CF_3). ^{19}F{H} NMR (376 MHz, DMSO-d_6) [ppm]: δ = −69.70 (s, 3F, CF_3). Mass: [$C_7H_{11}F_3N_2O_2Na^+$] calculated: 235.07 g mol^{-1}, measured: 235.07 g mol^{-1}.

Synthesis of 3-(trifluoromethyl)adiponitrile (ADN-CF_3).—3-(Trifluoromethyl)hexanediamide (3) (11.2 g, 0.053 mol, 1 eq.) and phosphorus pentoxide (37.5 g, 0.264 mol, 5 eq.) in abs. acetonitrile (130 mL) were refluxed under argon at 100°C for 24 h. After distillation and drying under vacuum ($\sim 10^{-3}$ mbar), 3-(trifluoromethyl)adiponitrile (**ADN-CF_3**) was received as colorless liquid (yield = 7.6 g, 0.043 mol, 81%). ^{1}H NMR (400 MHz, $CDCl_3$) [ppm]: 2.77-2.52 (m, 5H, CH_2CH_2CH), 2.17/ 2.04 (2x sext, $J_{H\text{-}F}$ = 7.2 Hz/ 7.1 Hz, 2 × 1H, CH_2). ^{19}F NMR (376 MHz, $CDCl_3$) [ppm]: δ = −70.86 (d, $J_{F\text{-}H}$ = 7.2 Hz, 3F, CF_3). ^{19}F{H} NMR (376 MHz, $CDCl_3$) [ppm]: δ = −70.86 (s, 3F, CF_3). Mass: [$C_7H_7F_3N_2Na^+$] calculated: 199.05 g mol^{-1}, measured: 199.05 g mol^{-1}.

Synthesis of aluminum bis(trifluoromethylsulfonyl)imide.—Bis(trifluoromethylsulfonyl)imide (2.0 g, 0.007 mol, 1 eq.) was dissolved in double-distilled water (9 mL). Aluminum foil was washed several times with ethanol, dried under vacuum ($\sim 10^{-3}$ mbar) and cut into pieces in the dry room (water content below 30 ppm and a temperature of approx. 20°C). After adding the aluminum pieces (0.3 g, 0.011 mol, 1.6 eq.) to the aqueous solution, the solution was refluxed at 110°C for 8 h. The residual aluminum was filtered off and the filtrate was concentrated using a rotary evaporator. The residue was dried at 140°C and 0.001 mbar for 24 h. Aluminum bis(trifluoromethylsulfonyl)imide was obtained as a white solid (yield = 1.6 g, 0.005 mol, 71%). ^{13}C NMR (101 MHz, DMSO-d_6) [ppm]: 119.54 (q, $J_{C\text{-}F}$ = 321.8 Hz, 2x CF_3). ^{19}F NMR (376 MHz, DMSO-d_6) [ppm]: δ = −78.77 (s, 6F, 2x CF_3)[ppm]. Mass: [$C_2F_6NO_4S_2$] calculated: 279.92 g mol^{-1}, measured: 279.92 g mol^{-1}.

Cyclic voltammetry measurements.—The CV measurements were performed with a VMP3 (BioLogic Science Instruments) in the potential range of 3–5 V vs. Li/Li^+ with a scan rate of 0.5 mV s^{-1} at 20°C. A three-electrode Swagelok cell was used with aluminum (Ø 12 mm) as working electrode, lithium metal as counter (Ø 12 mm) and reference (Ø 5 mm) electrode, and Whatman glass microfiber separator (Grade GF/D) wetted with 200 µL electrolyte.

Chronocoulometry measurements.—Chronocoulometry measurements were performed with a VMP3 (BioLogic Science Instruments). After linearly increasing the potential from OCP to 5 V vs. Li/Li^+ within 1 h, the potential was kept at 5 V vs. Li/Li^+ for 72 h at 20°C. In a three-electrode Swagelok cell, aluminum (Ø 12 mm) served as working electrode, and lithium metal as counter (Ø 12 mm) and reference (Ø 5 mm) electrode. The Whatman glass microfiber separator (Grade GF/D) was wetted with 200 µL electrolyte.

SEM analysis.—SEM analysis was performed using a Carl Zeiss AURIGA SEM microscope (Carl Zeiss Microscopy GmbH) to analyze the surface morphology of the aluminum working electrode after the chronocoulometry experiment. The aluminum was removed from the cell in an argon-filled glove box and washed three times with DMC (500 µL) (BASF, battery grade). The samples were transferred into the instrument chamber without air contact.

XPS analysis.—XPS measurements were performed with an AXIS Ultra DLD (Kratos, UK) spectrometer with a monochromatic Al K_α (1486.6 eV) source. The cells were disassembled in an argon-filled glove box, and the aluminum was removed and washed three times

with DMC (500 µL) (BASF, battery grade). The samples were transferred into the instrument chamber without air contact and kept under reduced pressure ($<10^{-9}$ mbar) for 12h. The X-ray gun was operated at 12 kV accelerating voltage and 10 mA filament current, whereas a pass energy (PE) of 120 eV was applied. For each sample, three data points with lateral resolution of 700 × 300 mm were taken and arithmetically averaged. Data analysis was performed with CasaXPS software (Version 2.3.16 PR 1.6, Casa Software Ltd., U.K.) were the C 1s C-H/C-C peak was chosen as the internal standard for the binding energy (BE, 284.5 eV) calibration.

Permittivity measurements.—Permittivity measurements were carried out by means of an ALPHA DCM-470 permittivity meter (Zadow Electronics) in a dry room with a water content below 30 ppm and a temperature of approx. 20°C. The measurement was based on the determination of a phase angle shift from the current response of an applied AC voltage of 470 kHz.

Impedance measurements.—Electrolyte resistances were measured using a conductivity cell with parallel plates of platinized platinum connected to a VMP3 (BioLogic Science Instruments). The frequency was scanned from 1 kHz to 1 Hz. The resistances were determined by linearly fitting the impedance curves in the Nyquist plot and determining the intercepts with the real axis using ZView 3.2.

Viscosity measurements.—Viscosity measurements were performed with an Anton Paar MCR 301 rheometer in a dry room (water content below 30 ppm). The device was equipped with a temperature system CTD 450 and a CP50-0.5/TG measuring system with a diameter of 49.947 mm, a cone angle of 0.473° and a distance of 68 µm between cone and lower plate. The viscosities were measured in a temperature range of −10°C–50°C in steps of 10°C and at 25°C. The shear rates were increased with increasing temperature from 3000 s^{-1} to 9000 s^{-1}.

Conductivity measurements.—Ionic conductivities were measured using a MCS 10 impedance-based conductivity meter (BioLogic) with an integrated frequency response analyzer and a temperature control unit. The device was calibrated before every measurement with a KCl standard solution at 25°C. The measurement was then performed from −20°C to 50°C in 5°C steps spaced by 20 min ramps.

PFG NMR measurements.—The self-diffusion coefficients of the electrolyte species were determined from PFG NMR analysis. All measurements were performed with a stimulated echo sequence at a Bruker AVANCE III 200 spectrometer using a Bruker Diff30 probe at 25.0°C (stabilized with ± 0.1°C), equipped with a 5 mm ^{7}Li/^{1}H or ^{19}F coil. In each case, the gradient strengths were varied from 5-1800 G cm^{-1}, with a gradient pulse length δ of 1 ms and a diffusion time Δ of 50 ms, recording 16 scans at relaxation delays of up to 60 s. The self-diffusion coefficients were derived from fitting peak intensities as a function of the gradient strength according to Equation 1:

$$I = I_0 \cdot e^{-D\cdot\gamma^2\cdot g^2\cdot\delta^2\cdot(\Delta-\frac{\delta}{3})} \quad [1]$$

where I, I_0, D and g are the observed intensity of the NMR signal, initial intensity, diffusion coefficient, and the applied gradient strength, respectively. The corresponding gyromagnetic ratio γ was set to $1.655\cdot10^3$ Hz G^{-1} and $4.006\cdot10^3$ Hz G^{-1} for ^{7}Li and ^{19}F. Preliminary data analysis was performed based on the Bruker Diff tool (Bruker Topspin 3.5 software) and then refined with the Origin 2016 program package.

Raman measurements.—Raman spectra were recorded with a Bruker VERTEX 70 spectrometer, equipped with a RAM II Raman module and Nd:YAG laser with a wavelength of 1064 nm and power output of 300 mW. 1000 scans were acquired at a resolution of 2 cm^{-1}, all spectra were stored in the wave number range of 0 cm^{-1} to 4000 cm^{-1}. The Bruker OPUS software was applied for the Raman measurements, while the Origin 2016 program package was utilized for data analysis or peak deconvolution.

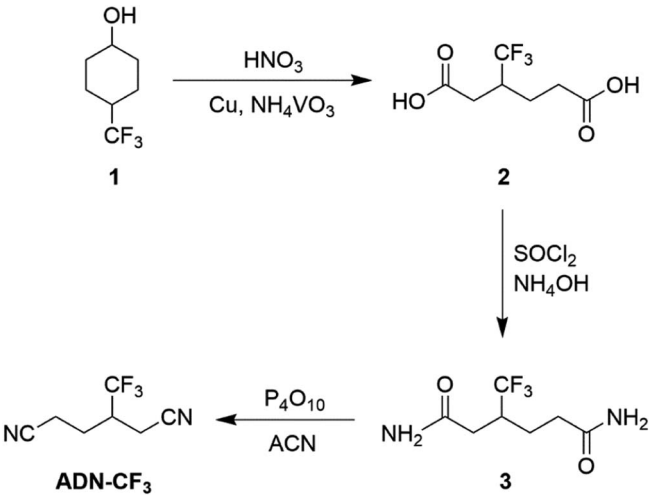

Figure 1. Synthesis route of 3-trifluoromethyladiponitrile (ADN-CF_3).

Results and Discussion

Electrochemical investigation of aluminum dissolution.—The aluminum dissolution behavior of electrolytes can be monitored with a number of complementary experiments.[24,29] By means of cyclic voltammetry, the cells are charged and discharged in a potential range of 3–5 V vs. Li/Li^+, where aluminum dissolution occurs whereas electrolyte oxidation can be excluded. This procedure approximates actual conditions of galvanostatic cycling in a lithium-ion cell, but cannot exactly simulate the potential profile of an NMC111 cathode.[45] In contrast, chronocoulometry displays the stability of the aluminum current collector at the upper potential for a defined period. The constant high potential stresses the aluminum much more, so that an absent current flow clearly indicates the absence of aluminum dissolution. This method simulates continuous charge, meaning rather abuse than real conditions in a lithium-ion cell, not considering the discharge process and its possible influence on the aluminum dissolution behavior. Another disadvantage of this experiment refers to the contribution of the monitored electric charge to the dissolution process, as faradaic reactions that are not related to aluminum dissolution take place in the first hours leading to an increase of the electric charge flow and current density.[20] For this reason, both methods were applied, and the obtained results are shown in Figures 2 and 3.

During the aluminum dissolution process, the electrochemical force, resulting from polarization in the anodic direction, promotes formation of Al^{3+} ions so that the natural surface layer of aluminum oxide (Al_2O_3) on the aluminum electrode and subsequently the exposed aluminum metal are oxidized.[25,26] An electron release during oxidation indicates charge transfer and consequently current flow, hence current densities can be taken as a measure for aluminum dissolution. LiTFSI salt in combination with PC is known to cause aluminum current collector dissolution.[46] Therefore, maximum current densities of more than 0.8 mA cm^{-2} are expected in cyclic voltammetry and chronocoulometry experiments, thus reflecting strong aluminum dissolution. We denote current densities lower than 0.01 mA cm^{-2} as reduced aluminum dissolution and values between 0.01 and 0.8 mA cm^{-2} as moderate dissolution in CV and CC experiments. Here, 1 M LiTFSI in PC shows a maximum current density of 1.34 mA cm^{-2} in CV experiments and therefore the strongest aluminum dissolution of all considered electrolytes. Apparently, an increasing amount of ADN in a LiTFSI-containing PC-based electrolyte yields lower current densities. Using ADN as single solvent considerably reduces the maximum current density up to 0.10 mA cm^{-2}, however, it is still present, indicating moderate aluminum dissolution. Cells containing ADN-CF_3 show much lower current densities, so that 1 M LiTFSI in 70 wt-% ADN-CF_3 and 30 wt-% PC electrolytes lead to lower current densities (max. 0.04 mA cm^{-2}) than the ones containing 100

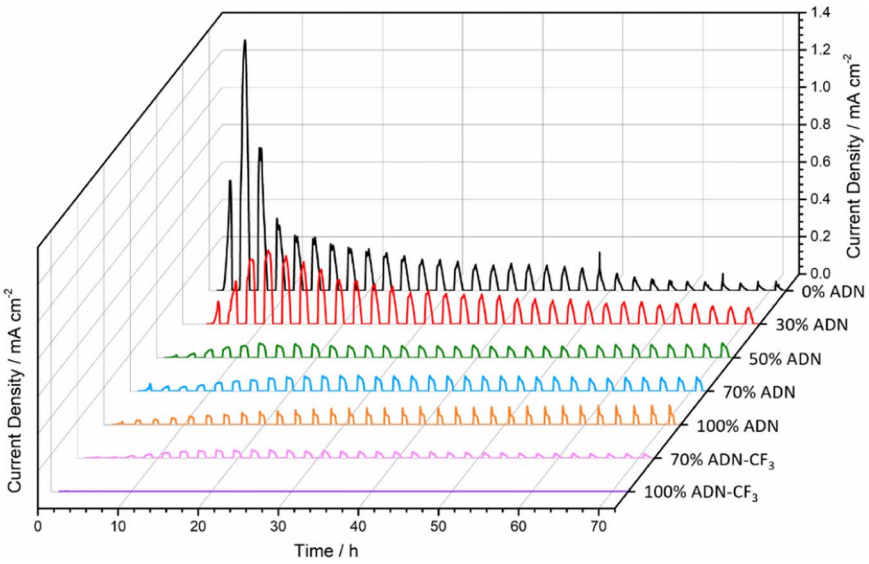

Figure 2. Current densities measured for 72 h at 20°C during cyclic voltammetry experiment between 3 and 5 V vs. Li/Li$^+$ conducted in Li/Al cells containing 1 M LiTFSI in x wt-% PC and (100-x) wt-% ADN or ADN-CF_3 with x = 0, 30, 50, 70, 100.

wt-% ADN. Cells with ADN-CF_3 as single solvent show no current densities at first view, both during CV and CC experiment. Zooming in and comparing the results of CC experiments with data obtained for cells containing 1 M $LiPF_6$ in EC/DMC (1:1 by wt), denoted as LP30, which show aluminum dissolution only to a minor extent because of $LiPF_6$ as conducting salt, reveals that a very slow current increase within 3 days occurs (Figure 3, bottom). An electrolyte, which fully suppresses aluminum dissolution, is only achieved upon addition of 1 wt-% LiBOB, a known additive for reduced aluminum dissolution.[23] ADN-CF_3 was identified as suitable solvent to reduce aluminum dissolution in the presence of LiTFSI, also in experiments with maximum strain, where comparable results to LP30 electrolyte were observed within 72 h; ADN-based electrolytes still lead to moderate aluminum dissolution.

Microscopic and spectroscopic characterization of aluminum surface.—A complete suppression of aluminum dissolution due to LiBOB addition can be monitored upon analysis of aluminum surfaces via SEM (Figure 4). The aluminum surface after 72 h CC with ADN-CF_3-based electrolyte containing 1 wt-% LiBOB looks similar to pristine aluminum, whereas the surface after treatment with 1 M LiTFSI in ADN-CF_3 electrolyte exhibits small pits and holes. In contrast, the holes after CC with ADN are much larger and with availability of PC still more pronounced (see SEM images in Figure S1). The observation that aluminum dissolution is not fully suppressed by ADN-CF_3 is attributed to the fact that no effective passivation layer is formed from electrolyte components or decomposition products, and that the natural surface layer of Al_2O_3 on pristine aluminum is destroyed, at least slowly. This leads to the suggestion that the typical mechanism for aluminum dissolution occurs, where $TFSI^-$ anions react with Al_2O_3 to form $Al(TFSI)_x$ species, which then diffuse from the aluminum electrode to the bulk electrolyte, cf. Ref. 20.

After the Al_2O_3 layer had disappeared, aluminum dissolution started at high potentials.[25] XPS analysis of selected aluminum electrodes was performed after treatment at 5 V vs. Li/Li$^+$ for 24 h in order to understand why aluminum dissolution is slowed down in the presence of ADN and ADN-CF_3. Peak areas are depicted in Table I.

The Al 2p spectrum (Figure 5, left) shows a decrease of the Al and Al_2O_3 peaks when ADN and ADN-CF_3 are used as solvents indicating formation of a surface layer, as Abu-Lebdeh et al.[31] proposed in 2009 with 1 M LiTFSI in ADN electrolyte, suggesting a passivation layer by Al^{3+} and $TFSI^-$ ions or by cyano groups of the nitriles through their lone electron pair. The N 1s spectrum (Figure 5, middle) reveals that CN groups are located on the aluminum surface. The C 1s spectrum (Figure 5, right) shows an increased amount of CF_3 with ADN-CF_3 (6.8 at.-%) compared to ADN (4.6 at.-%). However, it cannot be stated, whether the peak growth is due to increased $TFSI^-$ deposition or if the CF_3 group of the ADN-CF_3 molecule is also part of the surface.

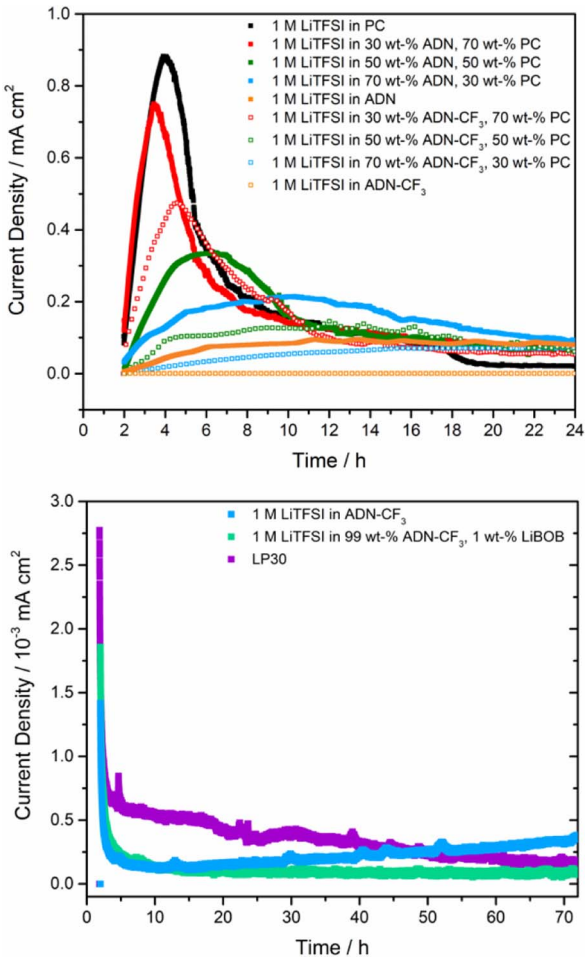

Figure 3. Current densities measured for 24 h (top) or 72 h (bottom) at 20°C when a constant potential of 5 V vs. Li/Li$^+$ is applied to a Li/Al cell containing 1 M LiTFSI in x wt-% PC and (100-x) wt-% ADN or ADN-CF_3 with x = 0, 30, 50, 70, 100. Additionally, LP30 and 1 M LiTFSI in 99 wt-% ADN-CF_3 and 1 wt-% LiBOB were used as electrolytes (bottom).

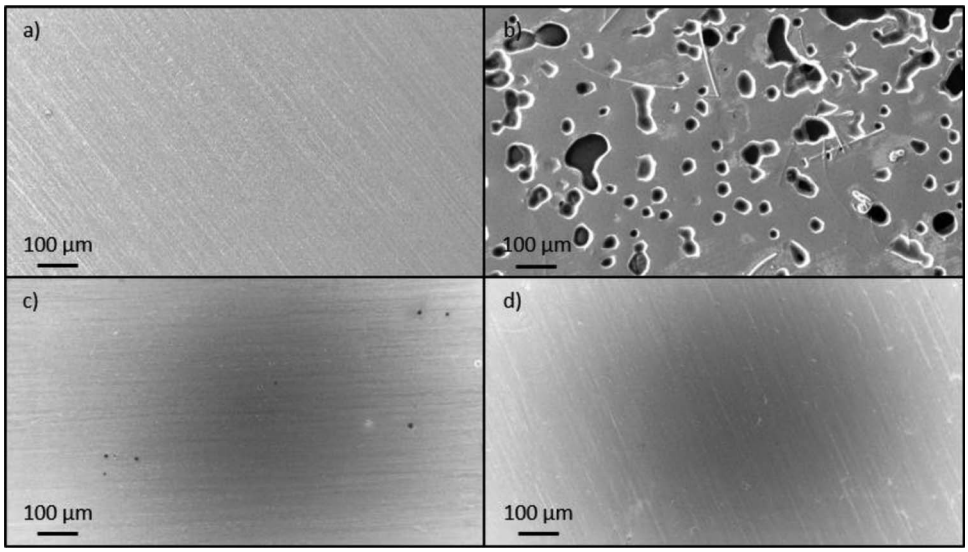

Figure 4. SEM images of aluminum electrodes with 100x magnification. a) pristine aluminum, b)-d) after chronocoulometry experiment at 5 V vs. Li/Li^+ for 72 h: b) 1 M LiTFSI in ADN, c) 1 M LiTFSI in ADN-CF_3, d) 1 M LiTFSI in ADN-CF_3, 1 wt-% LiBOB.

Table I. Peak areas from XPS spectra representing the amount of Al_2O_3, Al, CN and CF_3 on the aluminum electrodes after chronocoulometry experiments at 5 V vs. Li/Li^+ for 24 h.

		Peak area/at.-%			
			Electrode after CC experiment with		
Spectrum	Peak	Pristine electrode	1 M LiTFSI in ADN	1 M LiTFSI in ADN-CF_3	1 M LiFSI in ADN-CF_3
Al 2p	**Al_2O_3**	19.4 ± 0.2	7.5 ± 0.6	7.9 ± 0.2	13.6 ± 0.2
	Al	6.5 ± 0.8	0.6 ± 0.2	0.9 ± 0.0	2.2 ± 0.1
N 1s	**CN**	—	4.6 ± 0.4	3.7 ± 0.8	2.2 ± 0.3
C 1s	**CF_3**	—	4.6 ± 0.1	6.8 ± 0.1	0.9 ± 0.4

Repeating the CC measurement with a conducting salt without CF_3 group can help to evaluate whether the CF_3 peak of the ADN-CF_3 molecule is overlapped by the CF_3 peak representing $TFSI^-$. LiFSI should be the salt of choice, as it is structurally similar to LiTFSI (both CF_3 groups are replaced by fluorine atoms), and also causes aluminum dissolution, even though the effect of FSI^- anions could be a bit stronger than of $TFSI^-$ anions.[47] The F 1s spectrum cannot be used for evaluation of CF_3 peaks, as FSI^- and $TFSI^-$ ions have similar binding energies. However, the C 1s spectrum reveals a small CF_3 peak with a peak area of 0.9 at.-% in absence of TFSI, which is, together with the fact that CN groups are present, indicative of the depletion of solvent molecules, although the aluminum was washed with DMC prior to XPS analysis. There is no clear evidence that the ADN-CF_3 molecule decomposes or that it behaves differently

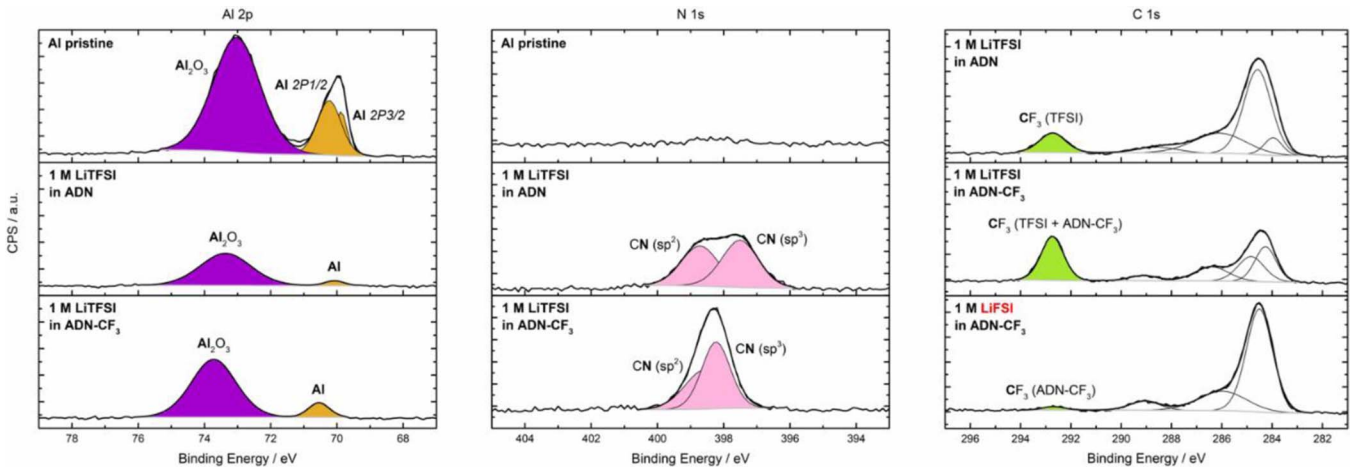

Figure 5. XPS spectra of pristine aluminum and aluminum electrodes after chronocoulometry experiments at 5 V vs. Li/Li^+ for 24 h with 1 M LiTFSI in ADN, 1 M LiTFSI in ADN-CF_3 and 1 M LiFSI in ADN-CF_3 as electrolytes. Left: Al 2p, middle: N 1s, right: C 1s spectrum.

Table II. Specific ionic conductivities at 20°C determined from impedance measurements before and 0.5, 1, 2, 5, 10 and 15 h after addition of 15 mg Al(TFSI)$_3$ to 500 µL of electrolyte solution. All data is accurate within ± 0.02 mS cm^{-1}.

	Specific ionic conductivities/mS cm^{-1}		
Time / h	1 M LiTFSI in PC	1 M LiTFSI in ADN	1 M LiTFSI in ADN-CF_3
0	4.60	2.13	0.31
0.5	3.76	1.94	0.29
1	3.68	1.92	0.29
2	3.66	1.90	0.29
5	3.62	1.85	0.28
10	3.60	1.82	0.28
15	3.60	1.80	0.28

than ADN. Nevertheless, it cannot be excluded that the increase in the intensity of CF_3 peaks in the C 1s spectrum is also a result of increased $TFSI^-$ deposition on the surface and not only because of the CF_3 group of ADN-CF_3 molecule. ICP-OES measurements of the washing solutions provide aluminum contents of 5.4 ppm and 2.5 ppm with an accuracy within ± 0.1 ppm for ADN and ADN-CF_3, respectively. Assuming that the same amount of electrolyte was washed off the aluminum electrodes, the obtained results indicate, that Al(TFSI)$_x$ species are more soluble in ADN-based electrolytes, thus they can readily be washed off. This conclusion is supported by the fact that the permittivity of ADN-CF_3 ($\varepsilon_r = 26.4$) is lower than that of ADN ($\varepsilon_r = 33.4$) and much lower than that of PC ($\varepsilon_r = 64.4$), indicating that salts and complexes like Al(TFSI)$_x$ have a reduced solubility in dinitriles. Therefore, the more pronounced CF_3 peak in the C 1s spectrum of electrodes after CC experiment with ADN-CF_3-based electrolytes also suggests increased $TFSI^-$ deposition on the surface.

Investigation of the solubility of Al(TFSI)$_3$.—The different solubility of Al(TFSI)$_3$ in PC-, ADN- and ADN-CF_3-based electrolytes can be demonstrated by impedance measurements. Assuming that Al(TFSI)$_3$ is the main product of aluminum dissolution, this compound was synthesized and 15 mg were added to 500 µL of PC- or dinitrile-based electrolytes. A similar experiment has already been performed by Krummacher et al.,[48] who investigated the solubility behavior of Al(TFSI)$_3$ in ADN and other unconventional solvents. The increase of resistances was monitored by electrochemical impedance spectroscopy (see Nyquist plots in Figure S2). Specific ionic conductivities κ were calculated by Equation 2 and are depicted in Table II.

$$R = \rho \cdot \frac{l}{A} = \rho \cdot C = \frac{1}{\kappa} \cdot C \qquad [2]$$

where R denotes the resistance of the ionic solution, determined by linearly fitting the plot and taking the intercept with the real axis. ρ is the resistivity, l the space between the plates, A the area of the plates and C the cell constant (1.059 cm^{-1}).

When Al(TFSI)$_3$ is added to the PC-based electrolyte, the resistance considerably increases up to a relative resistance of 128% after 15 h, as depicted in Figure 6. It seems as if the Al(TFSI)$_3$ salt addition slows down the ion transport, since the specific ionic conductivity decreases from 4.60 mS cm^{-1} to 3.60 mS cm^{-1}. When ADN is used as an electrolyte solvent, the resistance increases more slowly, attaining a relative resistance of 118% at the end of the experiment, whereas the resistance of ADN-CF_3-based electrolytes only increases up to 111% corresponding to a slight decrease of specific ionic conductivity from 0.31 mS cm^{-1} to 0.28 mS cm^{-1}. The results reflect the ratio of permittivities, showing that PC-based electrolytes much better dissolve Al(TFSI)$_3$ due to the high relative permittivity of PC ($\varepsilon_r = 64.4$), avoiding Al(TFSI)$_x$ deposition on the aluminum surface. In comparison, dinitrile-based electrolytes hardly dissolve Al(TFSI)$_3$. Note that the dissolution of Al(TFSI)$_3$ in the ADN-CF_3-based electrolyte is slower than in the ADN-based electrolyte, suggesting that the formed passivation layer of Al(TFSI)$_x$ on the aluminum surface with ADN-CF_3 is more stable and that the aluminum current collector dissolution is slowed down.

Ionic interactions and transport properties.—The solubility of salts in solvents is not only the result of relative permittivities (which is a physical property of the solvent), but considering the work of Yamada et al.,[26] the ionic interactions in the electrolyte are also of particular importance. They suggested for highly concentrated electrolytes that all solvent molecules are coordinated to Li^+ ions, so that there is no "free" solvent and the Al(FSI)$_x$ or Al(TFSI)$_x$ complexes are hardly dissolved. They stated that more solvent-Li^+ coordination should lead to less aluminum dissolution. Moreover, Li^+-FSI^- coordination is stronger, resulting in less formation of Al(FSI)$_x$, thus anions and solvents competitively coordinate Li^+. The coordination behavior of the involved species in the considered PC- and dinitrile-based electrolytes was derived from Raman measurements and analysis. However, solvent-$TFSI^-$ interactions were not considered since MD simulations would be required to fully elucidate the impact of the solvation shell structures.[39] The Raman peak at ~740 cm^{-1} is found to be the most suitable peak for analyzing Li^+-$TFSI^-$ interactions.[49–53] While no shift is observed for "free" $TFSI^-$, the peak reflecting coordinated $TFSI^-$ (ion pairs or aggregates) is shifted to higher wavenumbers (~748 cm^{-1}). In Figure 7, it can be seen that Li^+-$TFSI^-$ coordination is increased when ADN and particularly ADN-CF_3 are used as electrolyte solvents instead of PC, as the peak belonging to coordinated $TFSI^-$ is more pronounced (Figure 7, top). After deconvolution of the Raman spectra, the average coordination numbers n were determined by multiplying the ratio of the ligand (e.g., $TFSI^-$, CN^- or PC)

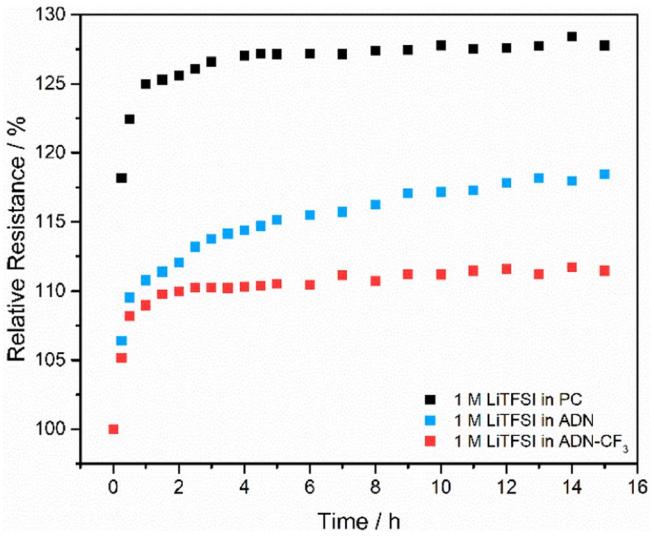

Figure 6. Relative resistances of 1 M LiTFSI in PC, ADN and ADN-CF_3 electrolytes recorded for 15 h after addition of 15 mg Al(TFSI)$_3$ to 500 µL of electrolyte solution at 20°C.

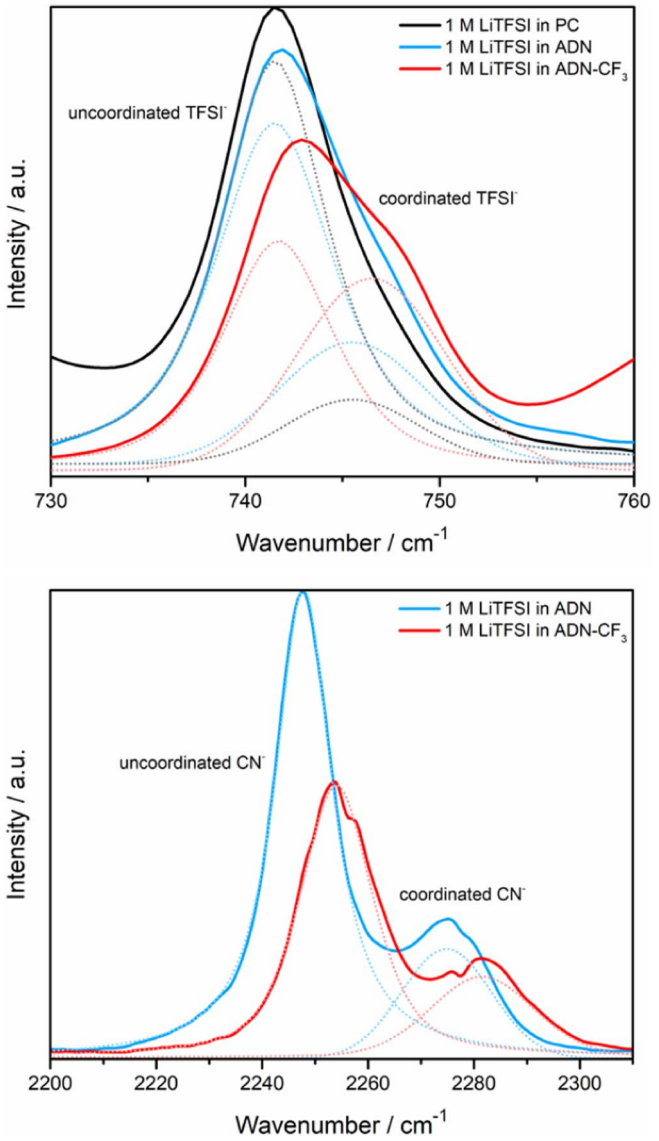

Figure 7. Raman spectra of 1 M LiTFSI in PC, ADN and ADN-CF_3 in the wavenumber range of 730–760 cm^{-1} (top) and 2200–2310 cm^{-1} (bottom) at 25°C. The dashed lines represent the peaks after deconvolution.

concentration c_{Ligand} and the Li^+ concentration c_{Li^+} with the ratio of the integrated peak areas according to Equation 3, where A_{coord} is the peak area attributed to the coordinating ligand, whereas A_{free} describes the peak area of "free" $TFSI^-$, CN^- or PC. The equation can be applied if we assume that coordinated and "free" ligands have comparable Raman scattering coefficients and that each ligand coordinates to a single Li^+ cation only.[50] The latter was verified by Molecular Dynamics (MD) simulations for ionic liquid/carbonate solvent electrolyte blends, where the fraction of ligand molecules coordinating to two lithium ions simultaneously only amounts to a few percent.[54]

$$n = \frac{c_{Ligand}}{c_{Li^+}} \frac{A_{coord}}{A_{coord} + A_{free}} \quad [3]$$

The calculated coordination numbers for $TFSI^-$ anions reveal an only moderate coordination to Li^+ cations in the considered electrolytes, i.e. 0.1, 0.3 and 0.5 $TFSI^-$ per Li^+ with PC, ADN and ADN-CF_3 as solvents, respectively. However, the increased Li^+-$TFSI^-$ coordination is also recognizable in the coordination numbers, however only slightly. The fact that the peak representing coordinated $TFSI^-$ is shifted to higher wavenumbers when a CF_3 group is present in the structure, i.e. from 745.4 cm^{-1} for ADN to 746.4 cm^{-1} for ADN-CF_3, reveals that the interaction between Li^+ and $TFSI^-$ is strengthened.

The Li^+-CN coordination can be analyzed on the basis of Raman peaks at ~2250 cm^{-1} and 2278 cm^{-1} for "free" CN^- ions and coordinated CN^-, respectively. The results reveal that Li^+ is on average surrounded by 2.8 CN groups in case of ADN and 3 CN groups with ADN-CF_3 so that ADN and ADN-CF_3 seem to adopt mono-dentate coordination. Farhat et al.[37] calculated a comparable coordination number of 3.3 for ADN. They were able to show that four CN groups coordinate Li^+ at low lithium salt concentrations ($\leq$ 0.5 mol/L) and that the coordination number decreases with higher concentrations of the salt. The peak representing Li^+-CN coordination is, just as the Li^+-$TFSI^-$ peak, shifted to higher wavenumbers when ADN-CF_3 is used as electrolyte solvent. The shift from 2274.8 cm^{-1} for ADN to 2282.3 cm^{-1} for ADN-CF_3 indicates a stronger Li^+-CN interaction. The most possible complexes are therefore $Li(ADN)_3^+$ and $Li(ADN\text{-}CF_3)_3^+$, where the interaction between Li^+ and ADN-CF_3 is stronger. Due to increased Li^+-$TFSI^-$ interaction in the presence of ADN-CF_3, it can be stated that ion pairs such as $[Li(ADN\text{-}CF_3)_3^+][TFSI^-]$ are more favored than $[Li(ADN)_3^+][TFSI^-]$. This can be related to relative permittivities, as higher permittivities are known to increase ion dissociation[55] and therefore lower permittivities lead to pronounced complex formation. Furthermore, ion transport parameters such as viscosities are responsible for such a behavior, as described in the next paragraph. With regard to ionic interactions, dinitrile-based electrolytes resemble highly concentrated electrolytes, revealing an increased solvent-Li^+ coordination and a stronger Li^+-$TFSI^-$ coordination, thus reasoning less formation of $Al(TFSI)_x$ and hardly dissolution of $Al(TFSI)_3$ when all solvent molecules are coordinated to lithium.

Ionic interactions are closely linked to ionic transport expressed by ionic conductivities, viscosities and self-diffusion coefficients of the single species. The absolute values at 25°C are shown in Table III. The ionic conductivity of 0.31 mS cm^{-1} of 1 M LiTFSI in ADN-CF_3 electrolytes is comparatively small, whereas the corresponding ionic conductivity of the ADN-based electrolytes is seven times as high (2.13 mS cm^{-1} / Farhat et al.[37]: 2.3 mS cm^{-1}). The PC-based electrolytes exhibit with 4.60 mS cm^{-1} the highest value, which is comparable to the experimental result of Vogl et al.[56] The ionic conductivities are dominated by the viscosities, as the viscosity of the 1 M LiTFSI in ADN-CF_3 electrolyte (150.0 mPa s) is also seven times as high as the one of 1 M LiTFSI in ADN electrolyte (21.0 mPa s / Farhat et al.[37]: 20.99 mPa s). However, the viscosity is still in a moderate range and not as high as for highly viscous ionic liquid-based electrolytes, such as 1 M LiTFSI in $Pyr_{14}TFSI$ electrolyte with 409.1 mPa s at 25°C.[54] The PC-based electrolytes show with 8.1 mPa s the lowest viscosity. This behavior can be on the one hand attributed to the stronger dipole-dipole interactions in ADN-CF_3-based electrolytes and the stronger complexes formed with Li^+ and $TFSI^-$, on the other hand to the molar masses of the solvents, as they increase from 102.09 g mol^{-1} via 108.14 g mol^{-1} through to 176.14 g mol^{-1} for PC, ADN and ADN-CF_3, respectively. A higher molecular mass makes the solvent moving more slowly through the electrolyte solution. This is also recognizable in the self-diffusion coefficients of ADN-CF_3 determined from PFG NMR analysis, which are with $0.6 \cdot 10^{-11}$ m^2 s^{-1} rather low. $D(Li^+)$ and $D(TFSI^-)$ have the same values, indicating that all species in this electrolyte are hindered to move, all as a result of the high viscosity.

1 M LiTFSI in PC electrolyte reveals the highest self-diffusion coefficients, including a maximum diffusion coefficient of Li^+ of $7.5 \cdot 10^{-11}$ m^2 s^{-1}. The value is comparable to Li^+ diffusion coefficients of 1 M LiTFSI in 40 wt-% $Pyr_{14}TFSI$, 60 wt-% EC/DMC (1:1 by wt) electrolytes ($0.7 \cdot 10^{-10}$ m^2 s^{-1}).[54] The Li^+ ions move faster in electrolytes based on EC/DMC only, reflected by a self-diffusion coefficient of $1.7 \cdot 10^{-10}$ m^2 s^{-1} for 1 M LiTFSI in EC/DMC (1:1 by wt).[54] In the considered PC- and ADN-based electrolytes, the Li^+ ions are the slowest diffusing species, whereas the solvent is the fastest species. The fact that $D(TFSI^-)$ decreases from PC to ADN to ADN-CF_3 indicates that the $TFSI^-$ ions move only slowly to the aluminum electrode, so that the reaction with Al_2O_3 to $Al(TFSI)_x$ is also slowed down, in agreement with the observations before. In

Table III. Ionic conductivities and viscosities of the investigated electrolytes, 1 M LiTFSI in PC, 1 M LiTFSI in ADN and 1 M LiTFSI in ADN-CF_3, as well as the self-diffusion coefficients of all involved species ($TFSI^-$, Li^+, solvents) at 25°C. Ionic conductivities, viscosities and self-diffusion coefficients are accurate within ±0.02 mS·cm^{-1}, ±0.5 mPa s and ±0.2 10^{-11} m^2 s^{-1}, respectively.

Electrolyte (25°C)	1 M LiTFSI in PC	1 M LiTFSI in ADN	1 M LiTFSI in ADN-CF_3
σ [mS cm^{-1}]	4.60	2.13	0.31
η [mPa s]	8.1	21.0	150.0
D(TFSI$^-$) [10^{-11} m^2 s^{-1}]	10.4	4.0	0.6
D(Li$^+$) [10^{-11} m^2 s^{-1}]	7.5	3.7	0.6
D(solvent) [10^{-11} m^2 s^{-1}]	14.8	5.4	0.6

general, it can be said that strong ionic and molecular interactions in the electrolyte as well as a slower ion transport, especially due to high viscosities, are indicative of reduced aluminum dissolution, as three different electrolyte classes, dinitrile-based, ionic liquid-based and highly concentrated electrolytes, show the same characteristics with regard to interactions, ion transport and aluminum dissolution. As elevated temperatures are known to improve ionic transport properties (see the temperature dependent ionic conductivities and kinematic viscosities in Figures S3 and S4), they also accelerate the aluminum dissolution process. Meister et al.[29] elucidated the temperature dependence using IL-based electrolytes with LiTFSI and lithium fluorosulfonyl(trifluoromethylsulfonyl)imide (LiFTFSI) as conducting salts. They reported that not only the anodic stability of the electrolyte is shifted toward lower potentials at higher temperatures, but also the measured current densities are higher, while pit formation on the aluminum is increased with both imide salt-containing electrolytes. Moreover, they confirm that solvents with high relative permittivities lead to pronounced aluminum dissolution, whereas high oxidative stabilities of solvents may suppress the dissolution due to reduced formation of acidic decomposition products as well as the lower solubility of $Al(TFSI)_x$ or $Al(FTFSI)_x$ species. Considering the oxidative stabilities of the here investigated electrolytes, the estimated trend was observed: the oxidation potential against platinum increases by substituting electrolyte solvents from PC (~5.6 V vs. Li/Li$^+$) to ADN (~5.8 V vs. Li/Li$^+$) to ADN-CF_3 (>8 V vs. Li/Li$^+$) (see linear sweep voltammetry data in Figure S5). Hence, the introduction of the CF_3 group leads to an increase of oxidative stabilities of more than 2.2 V vs. Li/Li$^+$. The higher electrochemical stability of ADN and especially of ADN-CF_3 indicates reduced aluminum dissolution in dinitrile-based electrolytes, suggesting that the electrochemical behavior of solvents should not be disregarded. Here, the viscosity was presented as new key parameter for assessing electrolytes in terms of aluminum dissolution, which, in combination with the relative permittivity, affects the aluminum dissolution mechanism by changing the velocity of $TFSI^-$ diffusion and solubility of $Al(TFSI)_x$ salt. In Figure 8, the process is schematically represented: high viscosities and low relative permittivities of the solvent result in increased Li^+-$TFSI^-$ coordination as well as stronger solvent-Li^+ interactions. Pronounced complex formation leads to the fact that $TFSI^-$ ions move only slowly to the aluminum electrode slowing down the reaction from Al_2O_3 or Al metal to $Al(TFSI)_x$. Moreover, increased solvent-Li^+ coordination implies the absence of "free" solvent molecules and impedes dissolution of $Al(TFSI)_x$. Solvents with low viscosities and high relative permittivities, however, lead to less interactions between the present species and therefore allow for faster diffusion of $TFSI^-$ anions to the aluminum electrode. The presence of rather "free" solvent molecules facilitates the solubility of $Al(TFSI)_x$ species and consequently degradation of the aluminum electrode. In a previous contribution, we were able to demonstrate that the overall viscosity determines the achievable ionic conductivity of a liquid electrolyte,[54] revealing that the viscosity constitutes a highly significant parameter for the design of advanced electrolytes.

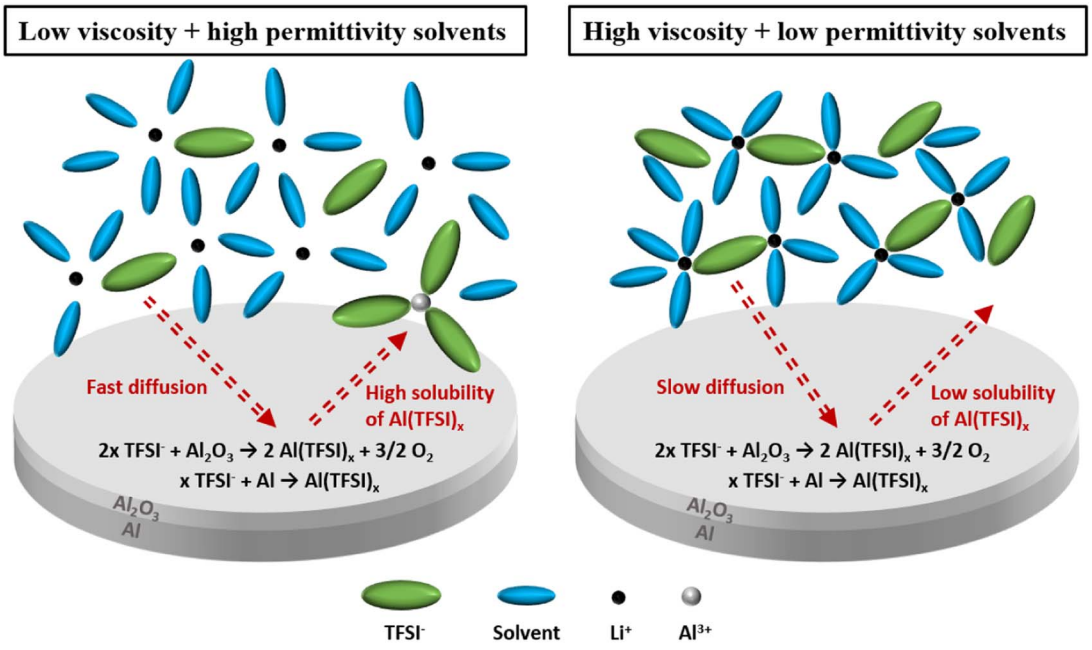

Figure 8. Schematic illustrations of the aluminum dissolution mechanism with low viscosity and high permittivity solvents (left) as well as high viscosity and low permittivity solvents (right).

Conclusions

In this work, we were able to highlight the relative permittivity of the considered solvents and the viscosity[54] of the entire electrolytes as key parameters for designing new electrolyte formulations, which have a positive impact on the aluminum dissolution behavior without prior decomposition of electrolyte components. Notably, ADN-CF_3 is identified as suitable electrolyte solvent to reduce aluminum dissolution in the presence of LiTFSI as conducting salt, considering that PC-based electrolytes yield pronounced aluminum dissolution (at max. current densities of 1.34 mA cm^{-2} during cyclic voltammetry experiment), whereas an addition of ADN as single solvent reduces the dissolution current densities to 0.10 mA cm^{-2}. Moreover, ADN-CF_3 as single solvent affords current densities below $4{\cdot}10^{-4}$ mA cm^{-2} so that the aluminum electrode showed only minimal pits, which could be even avoided by adding 1% LiBOB as electrolyte additive, suggesting that $Al(TFSI)_x$ species are formed upon reaction of $TFSI^-$ anions and Al_2O_3. XPS analysis confirmed that no protection layer is formed from decomposition products of ADN and ADN-CF_3, respectively. Rather, the oxidative stabilities and the relative permittivities of solvents, present ionic interactions and transport properties of the considered electrolytes appear particularly relevant. The oxidative stability increases from PC to ADN to ADN-CF_3, whereas the relative permittivity of ADN-CF_3 is lower compared to ADN and much lower than in case of PC, thereby leading to reduced ionic dissociation of lithium salts and lesser solubility of the $Al(TFSI)_x$ species. Notably, suitable electrolyte solvents that sufficiently suppress aluminum dissolution could be derived from high-viscosity solvents, indicating that dinitriles, particularly those with CF_3 groups that lead to higher molecular masses and significant changes in the electron density distribution, are highly suitable electrolyte solvents for lithium-ion batteries. This also holds due to their high thermal and anodic stabilities rendering them attractive for high voltage operation, despite that further efforts are required to establish appropriate cell systems to enable improved cycling with carbonaceous or graphitic electrodes. Hence, targeted design of electrolytes with low-permittivity solvents and high viscosities, resulting either from high-viscosity solvents or high concentrations of conducting salt, is rather promising for battery applications and is highly encouraged.

Acknowledgments

We thank Verena Naber for conducting the ICP-OES measurements, Tabea Mildenberger for technical support regarding electrolyte formulations and the state of NRW for funding (grant 433: ion conductors for highly effective energy storage devices).

ORCID

Isidora Cekic-Laskovic https://orcid.org/0000-0003-1116-1574
Gunther Brunklaus https://orcid.org/0000-0003-0030-1383

References

1. M. A. Hannan, M. M. Hoque, A. Hussain, Y. Yusof, and P. J. Ker, *IEEE Access*, **6**, 19362 (2018).
2. R. Schmuch, R. Wagner, G. Hörpel, T. Placke, and M. Winter, *Nat. Energy*, **3**, 267 (2018).
3. R. Wagner, N. Preschitschek, S. Passerini, J. Leker, and M. Winter, *J. Appl. Electrochem.*, **43**(5), 481 (2013).
4. T. Placke, R. Kloepsch, S. Dühnen, and M. Winter, *J. Solid State Electrochem.*, **21**(7), 1939 (2017).
5. X. Cao, X. He, J. Wang, H. Liu, S. Roser, B. R. Rad, M. Evertz, B. Streipert, J. Li, R. Wagner, M. Winter, and I. Cekic-Laskovic, *ACS Appl. Mater. Interfaces*, **8**(39), 25971 (2016).
6. P. G. Bruce, *Solid State Ionics*, **179**(21–26), 752 (2008).
7. S. Wiemers-Meyer, S. Jeremias, M. Winter, and S. Nowak, *Electrochim. Acta*, **222**, 1267 (2016).
8. S. Wiemers-Meyer, M. Winter, and S. Nowak, *Phys. Chem. Chem. Phys.*, **18**(38), 26595 (2016).
9. S. Zugmann, D. Moosbauer, M. Amereller, C. Schreiner, F. Wudy, R. Schmitz, R. Schmitz, P. Isken, C. Dippel, R. Müller, M. Kunze, A. Lex-Balducci, M. Winter, and H. J. Gores, *J. Power Sources*, **196**(3), 1417 (2011).
10. T. Böttcher, B. Duda, N. Kalinovich, O. Kazakova, M. Ponomarenko, K. Vlasov, M. Winter, and G. V. Röschenthaler, *Prog. Solid State Chem.*, **42**(4), 202 (2014).
11. R. W. Schmitz, P. Murmann, R. Schmitz, R. Müller, L. Krämer, J. Kasnatscheew, P. Isken, P. Niehoff, S. Nowak, G.-V. Röschenthaler, N. Ignatiev, P. Sartori, S. Passerini, M. Kunze, A. Lex-Balducci, C. Schreiner, I. Cekic-Laskovic, and M. Winter, *Prog. Solid State Chem.*, **42**(4), 65 (2014).
12. M. Amereller, T. Schedlbauer, D. Moosbauer, C. Schreiner, C. Stock, F. Wudy, S. Zugmann, H. Hammer, A. Maurer, R. M. Gschwind, H. D. Wiemhöfer, M. Winter, and H. J. Gores, *Prog. Solid State Chem.*, **42**, 39 (2014).
13. K. Kanamura, T. Okagawa, and Z. Takehara, *J. Power Sources*, **57**, 119 (1995).
14. B. Streipert, S. Röser, J. Kasnatscheew, P. Janßen, X. Cao, R. Wagner, I. Cekic-Laskovic, and M. Winter, *J. Electrochem. Soc.*, **164**(7), A1474 (2017).
15. J. W. Braithwaite, A. Gonzales, G. Nagasubramanian, S. J. Lucero, D. E. Peebles, J. A. Ohlhausen, and W. R. Cieslak, *J. Electrochem. Soc.*, **146**(2), 448 (1999).
16. X. Zhang, B. Winget, M. Doeff, J. W. Evans, and T. M. Devine, *J. Electrochem. Soc.*, **152**(11), B448 (2005).
17. K. Xu, *Chem. Rev.*, **104**, 4303 (2004).
18. D. W. McOwen, D. M. Seo, O. Borodin, J. Vatamanu, P. D. Boyle, and W. A. Henderson, *Energy Environ. Sci.*, **7**(1), 416 (2014).
19. H. Yang, K. Kwon, T. M. Devine, and J. W. Evans, *J. Electrochem. Soc.*, **147**(12), 4399 (2000).
20. E. Krämer, T. Schedlbauer, B. Hoffmann, L. Terborg, S. Nowak, H. J. Gores, S. Passerini, and M. Winter, *J. Electrochem. Soc.*, **160**(2), A356 (2013).
21. K. Kanamura, T. Umegaki, S. Shiraishi, M. Ohashi, and Z.-I. Takehara, *J. Electrochem. Soc.*, **149**(2), A185 (2002).
22. A. Hofmann, M. Schulz, V. Winkler, and T. Hanemann, *J. Electrochem. Soc.*, **161**(3), A431 (2014).
23. S. S. Zhang, *J. Power Sources*, **162**(2), 1379 (2006).
24. A. Heckmann, M. Krott, B. Streipert, S. Uhlenbruck, M. Winter, and T. Placke, *ChemPhysChem*, **18**(1), 156 (2017).
25. X. Wang, E. Yasukawa, and S. Mori, *Electrochim. Acta*, **45**, 2677 (2000).
26. Y. Yamada, C. H. Chiang, K. Sodeyama, J. Wang, Y. Tateyama, and A. Yamada, *ChemElectroChem*, **2**(11), 1687 (2015).
27. A. Heckmann, J. Thienenkamp, K. Beltrop, M. Winter, G. Brunklaus, and T. Placke, *Electrochim. Acta*, **260**, 514 (2018).
28. R.-S. Kühnel, M. Lübke, M. Winter, S. Passerini, and A. Balducci, *J. Power Sources*, **214**, 178 (2012).
29. P. Meister, X. Qi, R. Kloepsch, E. Krämer, B. Streipert, M. Winter, and T. Placke, *ChemSusChem*, **10**, 804 (2017).
30. E. Krämer, S. Passerini, and M. Winter, *ECS Electrochem. Lett.*, **1**(5), C9 (2012).
31. Y. Abu-Lebdeh and I. Davidson, *J. Electrochem. Soc.*, **156**(1), A60 (2009).
32. H. Duncan, N. Salem, and Y. Abu-Lebdeh, *J. Electrochem. Soc.*, **160**(6), A838 (2013).
33. M. Nagahama, N. Hasegawa, and S. Okada, *J. Electrochem. Soc.*, **157**(6), A748 (2010).
34. G. Y. Kim and J. R. Dahn, *J. Electrochem. Soc.*, **162**(3), A437 (2015).
35. Y. Abu-Lebdeh and I. Davidson, *J. Power Sources*, **189**(1), 576 (2009).
36. P. Isken, C. Dippel, R. Schmitz, R. W. Schmitz, M. Kunze, S. Passerini, M. Winter, and A. Lex-Balducci, *Electrochim. Acta*, **56**(22), 7530 (2011).
37. D. Farhat, F. Ghamouss, J. Maibach, K. Edstrom, and D. Lemordant, *ChemPhysChem*, **18**(10), 1333 (2017).
38. M. Winter, *Z. Phys. Chem.*, **223**, 1395 (2009).
39. A. N. Kirshnamoorthy, K. Oldiges, M. Winter, A. Heuer, I. Cekic-Laskovic, C. Holm, and J. Smiatek, *Phys. Chem. Chem. Phys.*, **20**, 25701 (2018).
40. B. Garcia and M. Armand, *J. Power Sources*, **132**(1–2), 206 (2004).
41. P. Murmann, X. Mönnighoff, N. von Aspern, P. Janssen, N. Kalinovich, M. Shevchuk, O. Kazakova, G.-V. Röschenthaler, I. Cekic-Laskovic, and M. Winter, *J. Electrochem. Soc.*, **163**(5), A751 (2016).
42. P. Murmann, N. von Aspern, P. Janssen, N. Kalinovich, M. Shevchuk, G.-V. Röschenthaler, M. Winter, and I. Cekic-Laskovic, *J. Electrochem. Soc.*, **165**(9), A1935 (2018).
43. I. M. Zalesskaya, A. N. Blakitnyi, E. P. Saenko, Y. A. Fialkov, and L. M. Yagupol'skii, *J. Org. Chem. USSR*, **16**, 1031 (1980).
44. M. J. Earle, B. J. Mcauley, A. Ramani, K. R. Seddon, and J. M. Thomson, US Pat., US6998497B2 (2006).
45. S. Brox, S. Röser, B. Streipert, S. Hildebrand, U. Rodehorst, X. Qi, R. Wagner, M. Winter, and I. Cekic-Laskovic, *ChemElectroChem*, **4**(2), 304 (2017).
46. S.-T. Myung, Y. Hitoshi, and Y.-K. Sun, *J. Mater. Chem.*, **21**(27), 9891 (2011).
47. R.-S. Kühnel and A. Balducci, *J. Power Sources*, **249** (2014).
48. J. Krummacher, L. H. Hess, and A. Balducci, *ChemSusChem*, (2017).
49. L. Aguilera, J. Scheers, and A. Matic, *Phys. Chem. Chem. Phys.*, **18**(36), 25458 (2016).
50. R.-S. Kühnel and A. Balducci, *J. Phys. Chem. C*, **118**(11), 5742 (2014).
51. M. Castriota, T. Caruso, R. G. Agostino, E. Cazzanelli, W. A. Henderson, and S. Passerini, *J. Phys. Chem. A*, **109**, 92 (2005).
52. D. Brouillette, D. E. Irish, N. J. Taylor, G. r. Perron, M. Odziemkowski, and J. E. Desnoyers, *Phys. Chem. Chem. Phys.*, **4**(24), 6063 (2002).
53. S. Menne, T. Vogl, and A. Balducci, *Phys. Chem. Chem. Phys.*, **16**(12), 5485 (2014).
54. K. Oldiges, D. Diddens, M. Ebrahiminia, J. B. Hooper, I. Cekic-Laskovic, A. Heuer, D. Bedrov, M. Winter, and G. Brunklaus, *Phys. Chem. Chem. Phys.*, **20**, 16579 (2018).
55. R. M. Fuoss and C. A. Kraus, *J. Am. Chem. Soc.*, **79**(13), 3304 (1957).
56. T. Vogl, S. Menne, and A. Balducci, *Phys. Chem. Chem. Phys.*, **16**(45), 25014 (2014).